Journal of Integrative Agriculture 2026, 25(8): 3282–3294

Available online at ScienceDirect

Journal of Integrative Agriculture



RESEARCH ARTICLE

Multi-omics analysis reveals dynamic metabolic and transcriptomic changes during potato tuber swelling

Jiangyue Long[1*], Wei Tan[1*], Chunzhi Zhang[2], Guangtao Zhu[1#], Zhong Zhang[2, 1#]

[1] *Yunnan Key Laboratory of Potato Biology/Engineering Research Center for Valorization of Unique Bio-Resources in Yunnan of Ministry of Education, School of Life Sciences, Yunnan Normal University/Southwest United Graduate School, Kunming 650500, China*

[2] *State Key Laboratory of Genome and Multi-omics Technologies/Shenzhen Branch, Guangdong Laboratory of Lingnan Modern Agriculture/Key Laboratory of Synthetic Biology, Ministry of Agriculture and Rural Affairs/Agricultural Genomics Institute at Shenzhen, Chinese Academy of Agricultural Sciences, Shenzhen 518120, China*

Highlights

- Metabolic and transcriptional dynamics during potato tuber development are revealed.
- Stage and genotype-specific metabolic patterns are identified in two genotypes.
- Novel genes involved in steroidal glycoalkaloid (SGA) and phenylpropanoid biosynthesis are discovered.
- *MYB113* positively regulates phenolic acid biosynthesis in tuber flesh.

Abstract

Potato is a vital global food source, yet the metabolic and transcriptional regulation governing tuber development and quality remains poorly understood. Here, we performed integrated metabolomic and transcriptomic analyses in wild and cultivated potato tubers, revealing dynamic and distinct metabolic accumulation patterns. The 849 metabolites exhibited 10 distinct temporal accumulation patterns, including six shared patterns between accessions and four genotype-specific patterns. The wild genotype exhibited an early decrease in lipids, followed by an increase in phenolic acids, whereas the cultivated genotype displayed an early increase in phenolic acids, accompanied by a decrease in some phenolic acids, amino acids, and flavonoids. A comparative analysis highlighted the cultivated genotype exhibited significantly lower levels of bitter steroidal glycoalkaloids (SGAs) but higher levels of beneficial flavonoids compared with its wild relative. Co-expression network analysis revealed 35 SGA-related and 57 phenylpropanoid-related genes that underlie metabolite dynamics. Notably, we functionally validated that the transcription factor *StMYB113* plays a previously unknown role in positively regulating phenolic acid biosynthesis in tuber flesh. Our work provides a comprehensive map of tuber metabolism and a valuable resource for accelerating the genetic improvement of key potato quality traits.

Keywords: potato, multi-omics, steroidal glycoalkaloid, phenylpropanoid, transcriptional regulation

1. Introduction

Potato (*Solanum tuberosum* L.) is a vital global food crop, serving as an essential source of carbohydrates and a diverse array of secondary metabolites, including steroidal glycoalkaloids (SGAs), flavonoids, and phenolic acids. These compounds, synthesized through complex biosynthetic pathways, are integral to plant defense and environmental adaptation. For instance, SGAs such as leptinine, commersonine, and demissine confer resistance to pathogens and herbivores in wild potato species (Tai *et al.* 2014; Cárdenas *et al.* 2019; Wolters *et al.* 2023), while glycosylated flavonoids enhance cold tolerance in *S. commersonii* under low-temperature stress (Zhu *et al.* 2023; Bao *et al.* 2024). Furthermore, many of these tuber metabolites exhibit bioactive properties, including antioxidant, anti-inflammatory, and anticancer effects, underscoring their potential to improve

Received 1 April 2025; Received in revised form 25 July 2025; Accepted 25 September 2025; Available online 31 December 2025
Jiangyue Long, E-mail: 2223120031@ynnu.edu.cn, Wei Tan, E-mail: 2223120009@ynnu.edu.cn; #Correspondence Guangtao Zhu, Tel: +86-871-65941387, E-mail: zhuguangtao@ynnu.edu.cn; Zhong Zhang, Tel: +86-755-23250158, E-mail: zhangzhong@caas.cn
*These authors contributed equally to this study.

© 2026 CAAS. Publishing services by Elsevier B.V. on behalf of KeAi Communications Co. Ltd. This is an open access article under the CC BY-NC-ND license (http://creativecommons.org/licenses/by-nc-nd/4.0/). Peer review under responsibility of Editorial Board of *Journal of Integrative Agriculture*.
doi: 10.1016/j.jia.2025.12.070

human health (Mattioli *et al*. 2020; Afnan *et al*. 2022; Al-Khayri *et al.* 2022; Lucier *et al.* 2024). Therefore, a deeper understanding of the biosynthesis and regulation of these metabolites is critical for enhancing tuber quality.

Significant progress has been made in identifying the key genes involved in these pathways. The biosynthesis of SGAs involves cholesterol synthesis, its conversion to solanidine, and subsequent glycosylation, mediated by *glycoalkaloid metabolism enzyme 1* (*GAME1*), *GAME2*, *GAME4*, *GAME6*, *GAME8*, *GAME11*, *GAME12*, *GAME15*, and others (Akiyama *et al.* 2023; Kang and Wang 2024). This process is governed by transcription factors (TFs) such as *GAME9*, *DELAY OF GERMINATION 1* (*DOG*), *ELONGATED HYPOCOTYL 5 (SlHY5)*, and *PHYTOCHROME INTERACTING FACTOR3 (SlPIF3)* (Cárdenas *et al.* 2016; Wang *et al.* 2018; Zhao X *et al.* 2023b). Concurrently, phenylpropanoids — predominantly, flavonoids and phenolic acids — are synthesized *via* a cascade, involving phenylalanine ammonia lyase (PAL), 4-coumarate:CoA ligase (4CL), cinnamate 4-hydroxylase (C4H), chalcone synthase (CHS), chalcone isomerase (CHI), flavanone 3-hydroxylase (F3H), dihydroflavonol 4-reductase (DFR), anthocyanidin synthase (ANS), *p*-coumarate-3-hydroxylase (C3H), and hydroxycinnamoyl transferase (HCT) (Deng and Lu 2017). The regulation of flavonoid metabolism is centrally controlled by myeloblastosis (MYB) TFs, which often interact with basic helix-loop-helix (bHLH) partners; for example, *StMYBA1* activates anthocyanin accumulation, a process enhanced by the StAN1-StbHLH1-StJAF13 complex (D'Amelia *et al*. 2014; Zhao X *et al.* 2023a; Du *et al.* 2025). However, despite these advancements, the dynamic metabolic shifts and the underlying transcriptional regulation networks during tuber development remain poorly understood.

To address this knowledge gap, recent studies have emphasized the utility of integrative metabolomic and transcriptomic analyses in unraveling plant biosynthetic pathways (Xu *et al.* 2020; Liu *et al.* 2023; Zhao L *et al.* 2023; Jia *et al.* 2024). Such multi-omics approaches have elucidated the mechanisms underlying the formation of flavors, pigments, and textures in various crops (Wang *et al*. 2022; Luo *et al.* 2024; Mao *et al.* 2024; Song *et al.* 2024). For instance, a pan-tissue metabolomic profile of tomatoes revealed systemic coordination between gene expression and metabolic activity across different developmental stages (Li *et al*. 2020). In potatoes, this strategy has already elucidated the chemical basis and regulatory mechanism of anthocyanin and carotenoid accumulation (Zhang *et al.* 2023), demonstrating its efficacy in uncovering novel metabolic networks.

In this study, we employed a multi-omics approach to systematically characterize the metabolic and transcriptional dynamics throughout potato tuber development. By tracking the temporal patterns of metabolite accumulation, we constructed a co-expression network that linked metabolites to gene expression, enabling the identification of key structural and regulatory genes. Notably, this integrative analysis uncovered a novel role for the transcription factor *StMYB113* in regulating phenolic acid biosynthesis in the tuber flesh. Our work illuminates the dynamic alterations in metabolic pathways during tuber development and reveals the underlying regulatory mechanisms. These findings provide critical metabolic and molecular insights for targeted improvements in tuber quality through potato breeding.

2. Materials and methods

2.1. Plant materials

Potato tubers sourced from a wild genotype, *S. candolleanum* PI458403, and a cultivated genotype, *S. tuberosum* 01-58 were grown in 35 cm×35 cm plots in an artificial climate chamber (Jiupo, Fujian, China) under conditions of 16 h light, 20°C, and 60% relative humidity (RH) during the vegetative growth, and 8 h light, 20°C, and 60% RH during tuberization. Tubers were sampled at seven time points (S1–S7) with an 8-day interval between each, starting approximately 70 days after planting. For metabolomic and transcriptomic profiling, the central pith of tubers from stages S3, S5, and S7 was excised, immediately frozen in liquid nitrogen, and stored. Three biological replicates were prepared for each sample to ensure data reliability.

2.2. Metabolome detection for tuber flesh

Lyophilized potato tissues were ground in a Mixer Mill (MM400; Retsch GmbH, Haan, Germany) at 30 Hz for 1.5 min. Approximately 100 mg of the resulting powder was extracted overnight at 4°C with 1.2 mL of 70% aqueous methanol. The extract was then filtered through a 0.22 μm membrane, and the filtrate was analyzed using an ultra-performance liquid chromatography-tandem mass spectrometry (UPLC-ESI-MS/MS) system (UPLC: Shimadzu, Tokyo, Japan; MS: Applied Biosystems, Waltham, USA), as previously described (Zhang *et al.* 2022). Separation was performed on Agilent SB-C18 (1.8 μm, 2.1 mm×100 mm). The mobile phase consisted of solvent A (0.1% formic acid in water) and solvent B (0.1% formic acid in acetonitrile) at a flow rate of 0.35 mL min^{-1} and a column temperature of 40°C. The elution gradient was: 95% A, 5% B at 0 min; a linear gradient to 5% A, 95% B over 9 min; held for 1 min; and returned to 95% A, 5% B in 0.1 min, followed by a 2.9 min re-equilibration. The injection volume was 4 μL. MS/MS conditions were: electrospray ionization temperature, 550°C; ion spray voltage, +5,500 V (positive mode) and –4,500 V (negative mode); and ion source gas I, gas II, and curtain gas pressures of 50, 60, and 25 psi, respectively. Each ion pair was scanned in the triple-quadrupole instrument using optimized collision energy and declustering potential values.

2.3. Metabolomics data analysis

Mass spectrometry data were qualitatively analyzed against the MWDB database. The Analyst 1.6.3 software was used to quantify the metabolite content for each chromatographic peak. For statistical analysis, principal component analysis (PCA) was performed using the prcomp package in R, with visualization by the factoextra package. K-means clustering was performed using the stats package (v4.2.0) in R. Differentially accumulated metabolites (DAMs) were identified using partial least squares discriminant analysis (PLS-DA), with significance defined as a fold change (FC)≥2 or ≤0.5, a *P*-value<0.05, and a variable importance in projection (VIP) score≥1.

2.4. RNA extraction and transcriptome sequencing

Total RNA was extracted from PI458403 and 01-58 tissues using TRIzol reagent (Invitrogen, Carlsbad, CA, USA). Sequencing was conducted on the MGISeq500 platform. Clean reads were aligned to the DM8.1 reference genome (http://www.bioinformaticslab.cn/pubs/dm8) using HISAT2 (Kim *et al.* 2019; Yang *et al.* 2023). Differentially expressed genes (DEGs) were identified from readcounts using DESeq2, based on a false discovery rate (FDR)≤0.05 and an absolute value of $\log_2$(FC)≥1. Kyoto Encyclopedia of Genes and Genomes (KEGG) pathway analysis was performed using OmicShare (https://www.omicshare.com/tools/). Transcriptome sequencing data are available in the SRA database under the accession number PRJNA1155134 (https://www.ncbi.nlm.nih.gov/sra/PRJNA1155134).

2.5. Weighted gene co-expression network analysis (WGCNA)

The gene co-expression network was constructed using the standard WGCNA procedure (Shannon *et al.* 2003; Langfelder and Horvath 2008). Genes with zero variance were removed, and only the top 50% of the remaining genes, ranked by median absolute deviation, were used for the analysis. A soft threshold of 18 was selected. The resulting weighted adjacency matrix was transformed into a topological overlap matrix to evaluate network connectivity. Genes were then grouped into modules based on their weighted correlation coefficients using hierarchical clustering.

2.6. Construction of expression vector and transformation into potato

The coding sequence of *StMYB113* was cloned from CIP705468 using primers, 5′-ATGAATATTGCCAAGTC ATTGGG-3′ (forward) and 5′-CTAATTAAATAGATTCCATAG GTCAATATCA-3′ (reverse). An overexpression (OE) vector, pCAMBIA2300-35S-*StMYB113*, was constructed and introduced into *Agrobacterium tumefaciens* strain GV3101. This vector was then transformed into CIP705468 stem segments, a genotype chosen for its low endogenous *StMYB113* expression and lack of pigment accumulation, as previously described (Ye *et al.* 2018). Transgenic plantlets harboring the target gene were selected on Murashige and Skoog (MS) medium containing 50 μg mL^{-1} kanamycin and 200 μg mL^{-1} Timentin. Positive transformants were confirmed using *NPT* II primers and fluorescence microscopy. Reverse-transcription quantitative PCR (RT-qPCR) was performed to quantify the expression levels of target genes. Transgenic and wild-type (WT) lines were grown in triplicate under greenhouse conditions. Tubers were harvested 110 days post-transplantation, and five similarly-sized tubers per line were selected for subsequent metabolomic and transcriptomic analyses.

3. Results

3.1. Dynamic development of potato tubers

To characterize tuber development, we investigated morphological changes in the wild (PI458403) and cultivated genotype (01-58) at seven time points (S1–S7) during tuber swelling development. The cultivated genotype, 01-58, exhibited substantial pigment accumulation in its tuber flesh from S2 onward, contrasting with the light-yellow flesh of PI458403 (Fig. 1-A). Both accessions showed a notable increase in tuber weight and width from S4 to S7 indicating a period of rapid tuber expansion (Fig. 1-B and C). Based on these observations, we defined three stages: early emergence (S1–S3), rapid growth (S4–S6), and ripening (S7), which corresponds to foliage senescence. Samples from the S3, S5, and S7 stages were subsequently selected for metabolic and transcriptomic profiling.

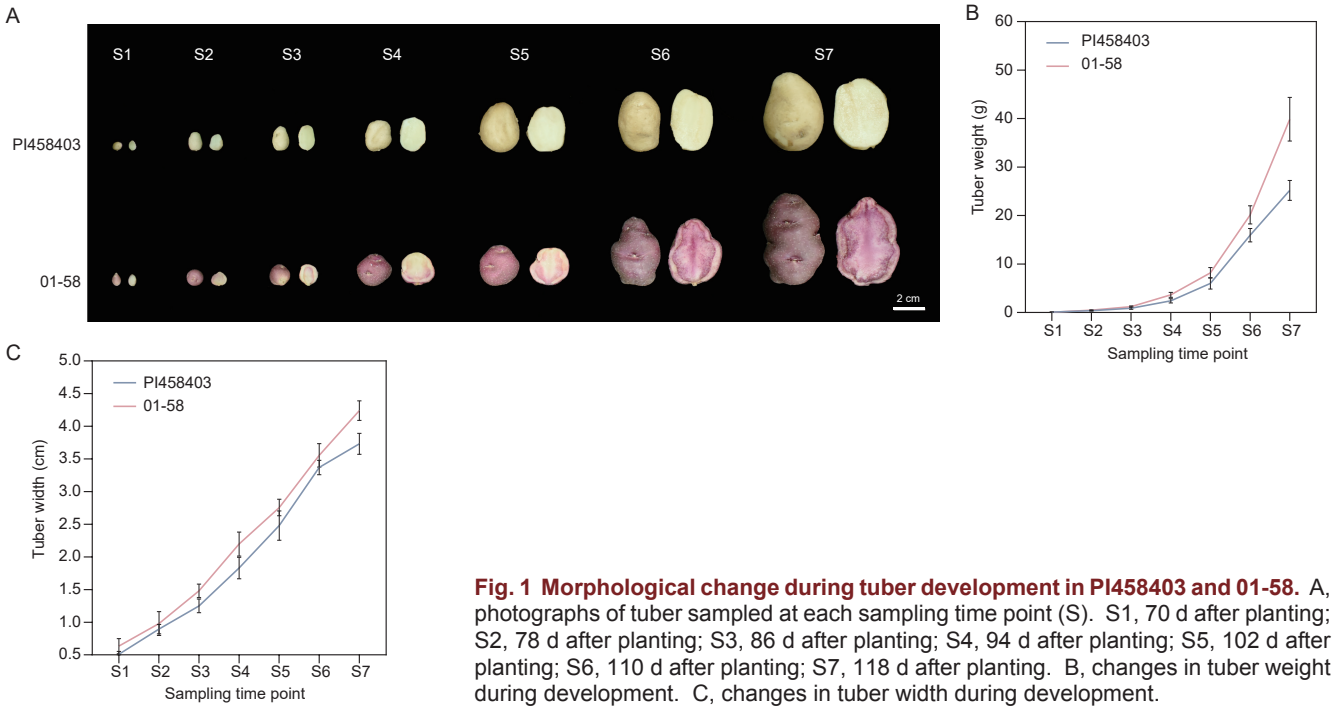


Fig. 1 Morphological change during tuber development in PI458403 and 01-58. A, photographs of tuber sampled at each sampling time point (S). S1, 70 d after planting; S2, 78 d after planting; S3, 86 d after planting; S4, 94 d after planting; S5, 102 d after planting; S6, 110 d after planting; S7, 118 d after planting. B, changes in tuber weight during development. C, changes in tuber width during development.

3.2. Multi-omics dataset construction

Metabolomic profiling of 18 samples (three stages×two accessions×three replicates), identified 849 metabolites (Appendix A). The composition was dominated by flavonoid (20.14%), phenolic acid (18.26%), lipid (14.61%), amino acid and derivative (10.72%), organic acid (9.07%), nucleotide (8.01%), SGA (7.18%), saccharide and alcohol (7.07%), phenolamide (3.30%), and vitamin (1.65%) (Fig. 2-A). A comparative heatmap analysis revealed notable differences in metabolite abundance across stages and genotypes; specifically, PI458403 accumulated significantly more SGAs and fewer flavonoids than 01-58 throughout development (Fig. 2-B). Correlation analysis confirmed strong consistency among the biological replicates (r>0.9, P<0.05; Appendix B), and PCA further validated the distinct metabolite profiles across developmental stages and genotypes (Appendix B).

For the transcriptome, sequencing generated 93.83 Gb of high-quality data, with 94.29% of the reads mapping to the reference genome (Appendix C). One biological replicate PI458403_S5_2 was excluded from the downstream analysis due to lower correlation coefficient relative to other replicates (Appendix B). Following this exclusion, PCA of the remaining samples confirmed high consistency (Appendix B).

3.3. Overview of metabolite accumulation patterns during tuber development

K-means clustering resolved metabolite accumulation into ten temporal patterns, six of which were common to both genotypes (Fig. 2-C; Appendix D). Classes 1 and

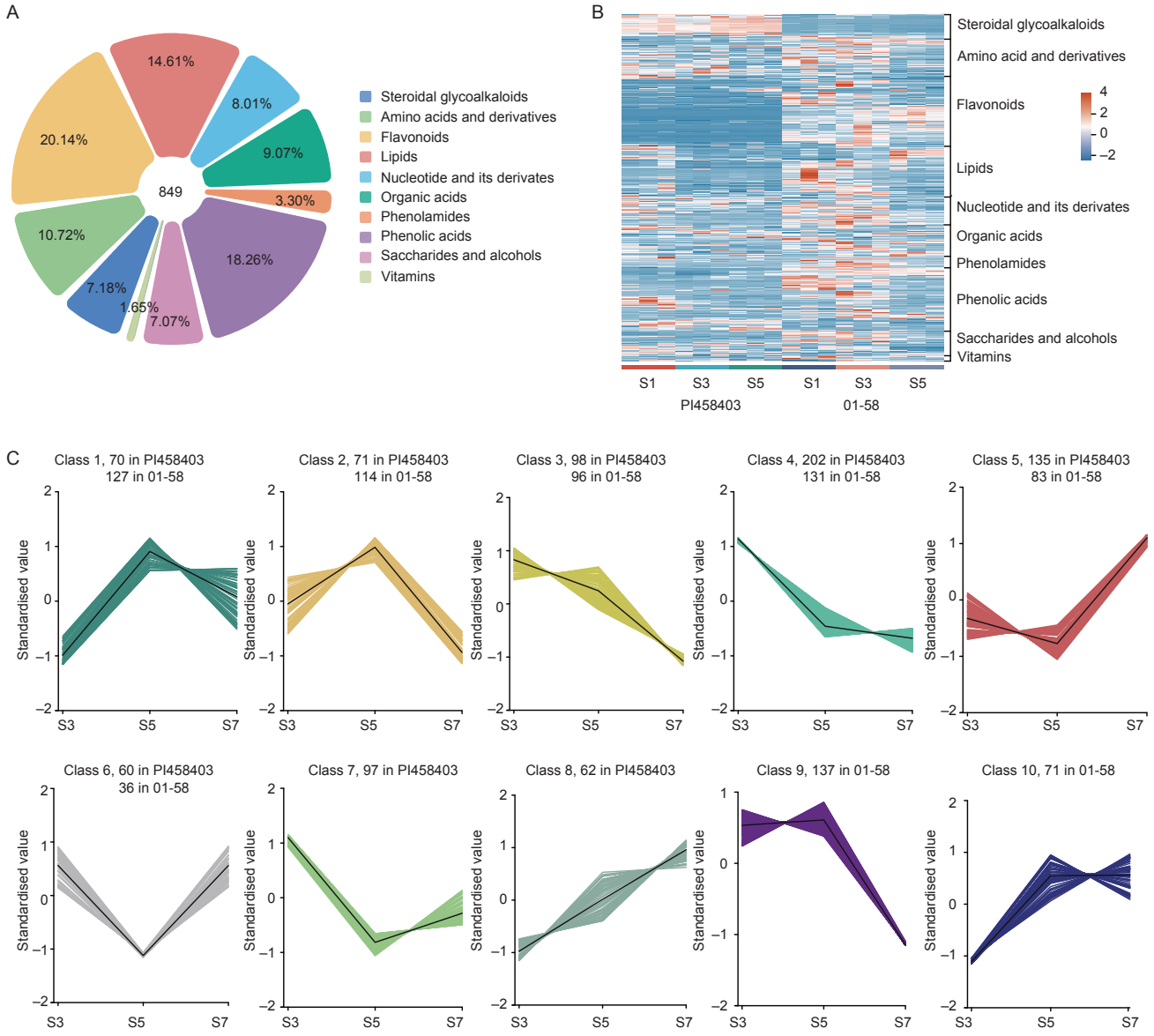


Fig. 2 Metabolome profiling of potato tuber. A, distribution of metabolites identified by liquid chromatography–tandem mass spectrometry (LC–MS/MS)-based detection, presented as a percentage of total metabolite numbers. B, heatmap illustrates fluctuation in metabolite abundance across sampling time points and samples. C, cluster of changing patterns of metabolites during tuber development. S3, 86 d after planting; S5, 102 d after planting; S7, 118 d after planting.

2, which increased from S3 to S5 before declining at S7, included 141 metabolites in PI458403 (predominantly amino acids, organic acids, and phenolic acids) and 241 in 01-58 (primarily phenolic acids, flavonoids, lipids, nucleotides, and amino acids). Among these, 21 metabolites were shared between the accessions, including six flavonoids, four alkaloids, and four organic acids. Classes 3 and 4 showed continuous decreases, encompassing 300 metabolites in PI458403 (phenolic acids, lipids, organic acids, amino acids, nucleotides, saccharides, alcohols, and flavonoids) and 227 metabolites in 01-58 (phenolic acids, lipids, organic acids, amino acids, nucleotides, saccharides, alcohols, and flavonoids). The metabolites shared between the accessions (n=83) included 18 lipids, 15 phenolic acids, 15 amino acids, and 14 nucleotides. Classes 5 and 6 showed a decrease from S3 to S5, followed by an increase at S7, comprising 195 metabolites in PI458403 (flavonoids, phenolic acids, and alkaloids) and 119 metabolites in 01-58 (lipids and flavonoids), with 16 flavonoids shared between the accessions.

Genotype-specific patterns were also observed. In PI458403, Class 7 (lipids, phenolic acids) declined then slightly increased, while Class 8 (flavonoids, phenolic acids) showed gradual accumulation. In 01-58, Class 9, rich in SGAs and amino acids, was stable before declining at S7. Class 10 (flavonoids, phenolic acids) progressively accumulated until S5 and then stabilized. Collectively, 636 metabolites in PI458403 and 587 metabolites in 01-58 demonstrated similar accumulation patterns, whereas 159 (PI458403) and 208 (01-58) metabolites exhibited genotype-specific template patterns. These results highlight dynamic and distinct metabolic changes in the wild and cultivated genotypes during tuber development.

3.4. Metabolic dynamics in potato tubers

We used PLS-DA to identify stage- and genotype-specific differentially accumulated metabolites (DAMs). Within PI458403, we identified 29 DAMs in the S5/S3 comparison and 25 in the S7/S5 comparison, with no DAMs common to both (Fig. 3-A and B). Notably, 13 lipids were downregulated in S5/S3, whereas 11 phenolic acids were upregulated in S7/S5 (Fig. 3-C). In contrast, 01-58 exhibited more pronounced changes, with 54 DAMs in S5/S3 and 60 in S7/S5, including 21 metabolites shared between the two comparisons (Fig. 3-A and B). Here, 15 phenolic acids were upregulated in S5/S3, while 12 phenolic acids and 8 flavonoids were downregulated in S7/S5 (Fig. 3-D).

A direct comparison between the genotypes identified 271 DAMs that distinguished 01-58 from PI458403, with 51 metabolites shared across all three stages (Fig. 3-A and E). These core DAMs included 21 SGAs, 21 flavonoids, and 6 phenolic acids. At all stages, 01-58 showed upregulated flavonoids and phenolic acids but downregulated SGAs compared to PI458403 (Fig. 3-F). This pattern reflects their distinct backgrounds whereas PI458403 maintained high levels of defensive SGAs, while the cultivated 01-58 accumulated flavonoids such as pelargonidin derivatives, consistent with its red flesh.

3.5. Transcriptional dynamics in potato tubers

Comparative transcriptomics revealed stage- and genotype-specific differences that correlated with the observed metabolite dynamics. In PI458403, we identified 333 DEGs at S5/S3 and 74 at S7/S5 (Appendix E), with 22 genes common to both comparisons (Appendices E and F). The S5/S3 DEGs were enriched in lipid metabolism pathways, consistent with downregulated lipid profiles, while S7/S5 DEGs were enriched in phenylpropanoid biosynthesis, aligning with the dynamics of phenolic acids (Appendix E). For 01-58, we identified 505 DEGs in S5/S3 and 1,147 in S7/S5 (Appendix E). KEGG analysis of S5/S3 DEGs showed enrichment of amino acid biosynthesis and downregulation of flavonoid pathways. By S7/S5, transcriptional activity shifted toward upregulated flavone/flavonol biosynthesis, mirroring the corresponding metabolite dynamics (Fig. 3-D).

Direct comparison between genotypes identified 4,114 (S3), 1,629 (S5), and 1,297 (S7) DEGs, with 537 DEGs shared across all stages (Appendix E). In all comparisons, KEGG analysis revealed that the steroid biosynthesis pathway was consistently downregulated in 01-58, while flavonoid biosynthesis was markedly upregulated, highlighting the distinct transcriptional programs governing the metabolism of the two accessions.

3.6. WGCNA reveals transcriptional modules governing metabolic biosynthesis

WGCNA of 21,585 genes identified 12 distinct co-expression modules (Appendix G). We correlated module expression with metabolite abundance, finding 225 metabolites strongly correlated (r^2≥0.8, P<0.05) with at least one module (Fig. 4-A; Appendix H). Two significant clusters emerged: module M7 showed strong correlations with 39 SGAs, while modules M1 and M3 were associated with 48 phenylpropanoids (45 flavonoids and 3 phenolic acids) (Fig. 4-A). Given their association with the primary metabolic differences observed, these modules were selected for further analysis. Overlapping module genes with DEGs from the stage/genotype comparisons yielded 353 candidate genes for M7 and a combined 2,529 for M1 and M3 (Fig. 4-B; Appendix I).

3.7. Transcriptional dynamics of SGA biosynthesis between accessions

Metabolomic analysis revealed a pronounced reduction in SGA levels in 01-58 compared to PI458403 at all developmental stages (Appendix J). To understand the underlying transcriptional mechanisms, we examined the expression of known structural genes involved in SGA biosynthesis. A total of 14 genes in the cholesterol biosynthesis pathway, including *acetyl-CoA acetyltransferase 1* (*ACAT1*), *3-hydroxy-3-methylglutaryl-CoA synthase 1* (*HMGS1*), *3-hydroxy-3-methylglutaryl-CoA reductase 5* (*HMGR5*), *mevalonate kinase* (*MVK*), *farnesyl diphosphate synthase 2* (*FPPS2*), *squalene synthase 1* (*SQS1*), *squalene epoxidase 1* (*SQO1*), *SQO2*, *cycloartenol synthase 2* (*CAS2*), *sterol side chain reductase 2* (*SSR2*), *C-4 sterol methyl oxidase 3* (*SMO3*), *SMO4*, *C5-sterol dehydrogenase 2* (*C5-SD2*), and *7-dehydrocholesterol reductase 2* (*DWF5-2*),

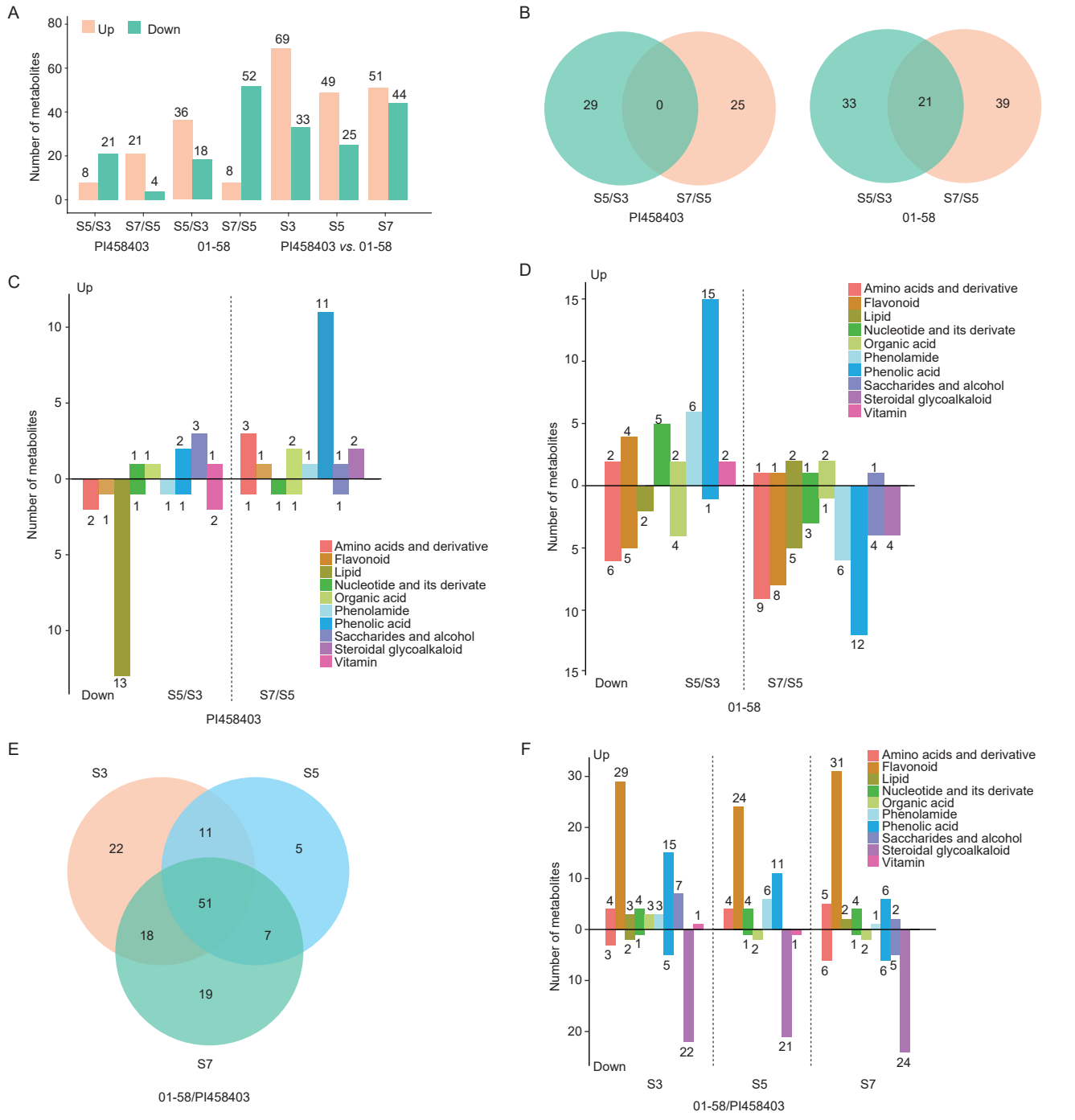


Fig. 3 Dynamic metabolite changes during tuber development in PI458403 and 01-58. A, identification of differentially accumulated metabolites (DAMs) through partial least squares discriminant analysis (PLS-DA) analysis, with fold change≥2 or ≤0.5 and VIP≥1. B, overlap of DAMs between S5/S3 and S7/S5 in PI458403 and 01-58. C and D, distribution of DAM counts across S5/S3 and S7/S5 in PI458403 (C) and 01-58 (D). E, overlap of DAMs across all stages comparing PI458403 to 01-58. F, distribution of DAM number for each stage between 01-58 and PI458403. S3, 86 d after planting; S5, 102 d after planting; S7, 118 d after planting.

and 11 genes in the subsequent conversion to solanidanes, *GAME1*, *GAME2*, *GAME6*, *GAME11*, *GAME15*, *GAME12*, *GAME4*, *GAME5*, and three *2-oxoglutarate-dependent dioxygenases-3/4/6* (*2ODD-3*/*4*/*6*), exhibited significantly higher expression in PI458403 than in 01-58 in at least two stages (FC≥2 and FDR<0.05) (Fig. 5-A) The coordinated downregulation of these structural genes in 01-58 aligns with its lower SGA accumulation and may reflect selection against a core transcriptional regulator during domestication.

To identify novel regulators, we analyzed the 35 candidate genes from module M7 (Fig. 5-B). These genes were identified based on their putative functional annotations for oxidation, reduction, acetylation, and glycosylation, which were acquired for biosynthesis/modification (Sonawane *et al.* 2022). Among these, 11 genes with putative roles in biosynthesis or modification, including *GAME12-like*,

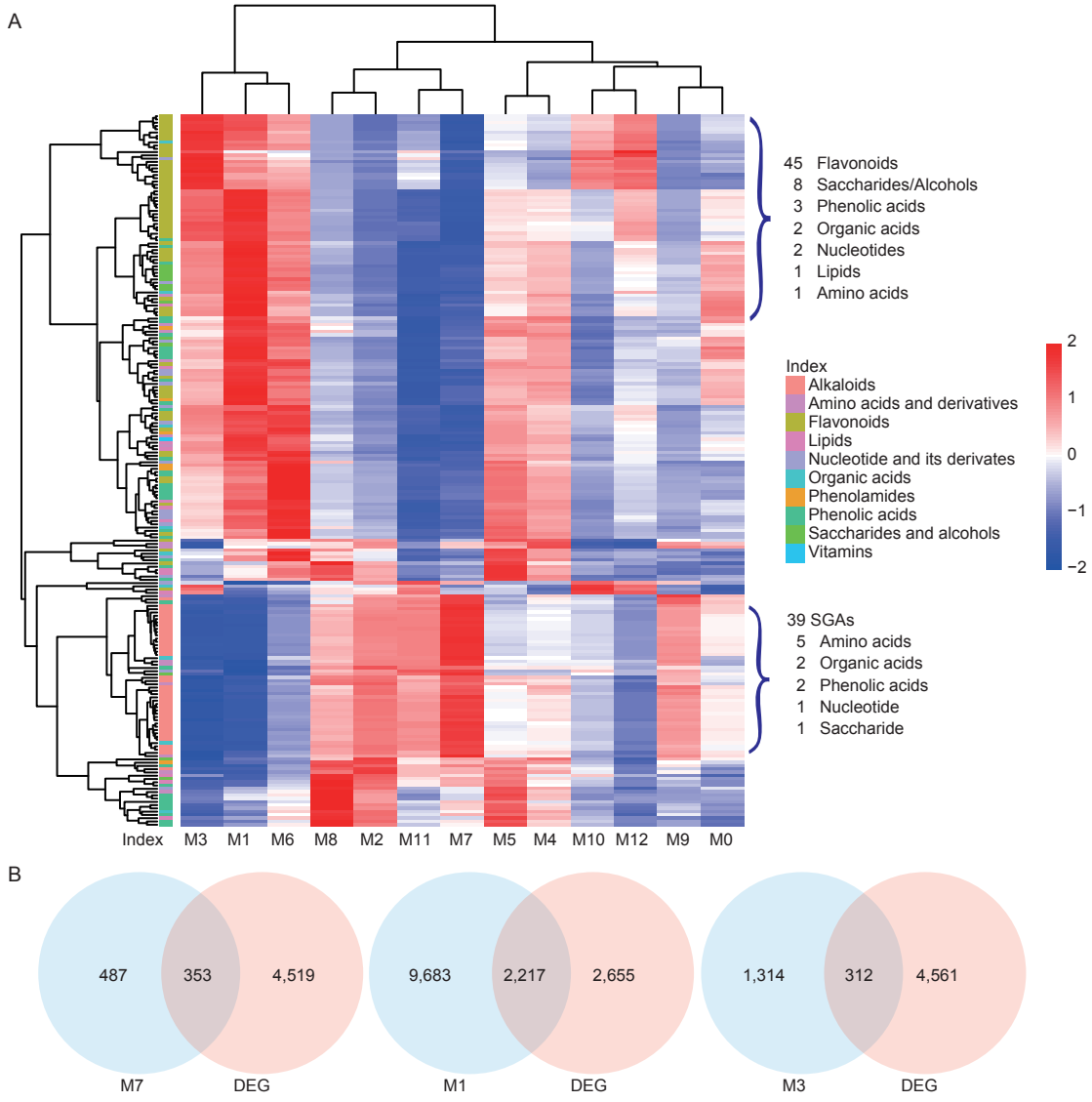


Fig. 4 Identification of candidate gene networks associated with the biosynthesis and regulatory mechanism of steroidal glycoalkaloids (SGAs) and phenylpropanoids through WGCNA. A, heatmap employed to cluster the correlation between metabolites and each individual module. B, overlap between genes enriched in modules and differentially expressed genes (DEGs) identified from stage-specific and genotype-specific comparisons.

2ODD7, *sterol 3-beta-glucosyltransferase* (*3βSD-UGT*), *cytochrome P450 71A* (*CYP71A1*), *CYP72A1/2/3*, *zeatin-O-glucosyltransferase 1/2/3* (*ZOG1/2/3*), and *BAHD acyltransferase* (*BAHD*), were substantially downregulated in 01-58 (Fig. 5-C; Appendix K). Additionally, the key regulator *GAME9* was significantly downregulated in 01-58 at S5 and S7, confirming its crucial role.

3.8. Transcriptional dynamics of phenylpropanoid metabolism

Metabolomic data revealed dynamic changes in phenylpropanoids in 01-58 during development and clear differences between the two accessions. Therefore, structural genes were identified based on their homology to the tomato phenylpropanoid biosynthesis genes (Appendix L). During the development of 01-58, *flavonoid 3′,5′-hydroxylase* (*F3′5′H*) exhibited marked downregulation from S3 to S5 (FC≤0.5 and FDR<0.05, Fig. 6-A), while *PAL1* was upregulated at S7 (FC≥2 and FDR<0.05; Fig. 6-A). However, other genes showed slight changes in expression, which aligned with the minimal metabolic flux alterations during tuber development at 01-58. Further comparison revealed that the pronounced accumulation of anthocyanins in 01-58 correlated with the sustained upregulation of 11 structural genes relative to PI458403 in at least two stages (FC≥2 and FDR<0.05; Fig. 6-A). These genes included *PAL9*, *CHS1/2/3*, *CHI3*, *F3H*, *F3′5′H*, *DFR*, *ANS*, *UDP-glycose flavonoid glycosyltransferase 1* (*UFGT1*), and *glutathione S-transferase* (*GST*). Upregulation of these genes enhanced the accumulation of pelargonidin derivatives, consistent with the higher levels of flavonoids in 01-58 compared with in PI458403. Conversely, *PAL2/3*, *C4H2*, *4CL2*, and *CHS4/5* were significantly suppressed in 01-58 relative to PI458403 (FC≤0.5 and FDR<0.05).

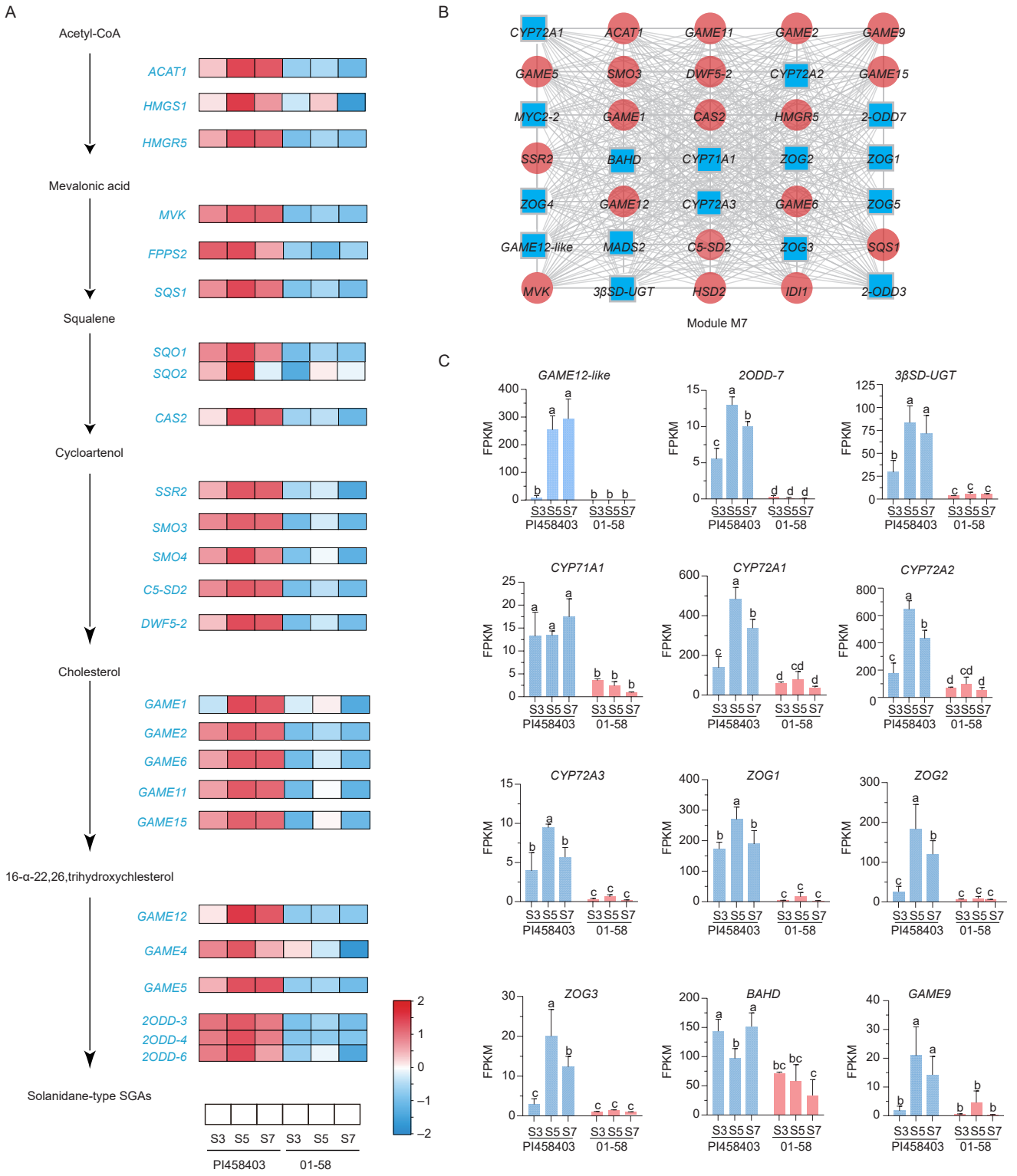


Fig. 5 Identification of candidate genes related to steroidal glycoalkaloids (SGAs) biosynthesis. A, heatmap illustration represents the expression levels of biosynthetic genes in SGA pathways. The color gradient, ranging from blue to red, visually conveys the transition from low to high expression levels of the FPKM values. B, candidate genes with putative function related to SGA biosynthesis and regulation. Red circles represent known genes identified previously, while blue rectangles indicate novel candidates identified in this study. C, expression changes of candidate differentially expressed genes related to SGA biosynthesis and regulation identified from module M7. S3, 86 d after planting; S5, 102 d after planting; S7, 118 d after planting. Data are mean±SD (n=3). The letters denote the distinctions in mean gene expression across samples, as determined through Tukey's test.

To identify candidate regulators, we characterized 39 TFs enriched in modules M1 and M3, spanning families, including AP2-like ethylene-responsive transcription factor (AP2), B3 domain-containing protein (B3), basic helix loop helix domain

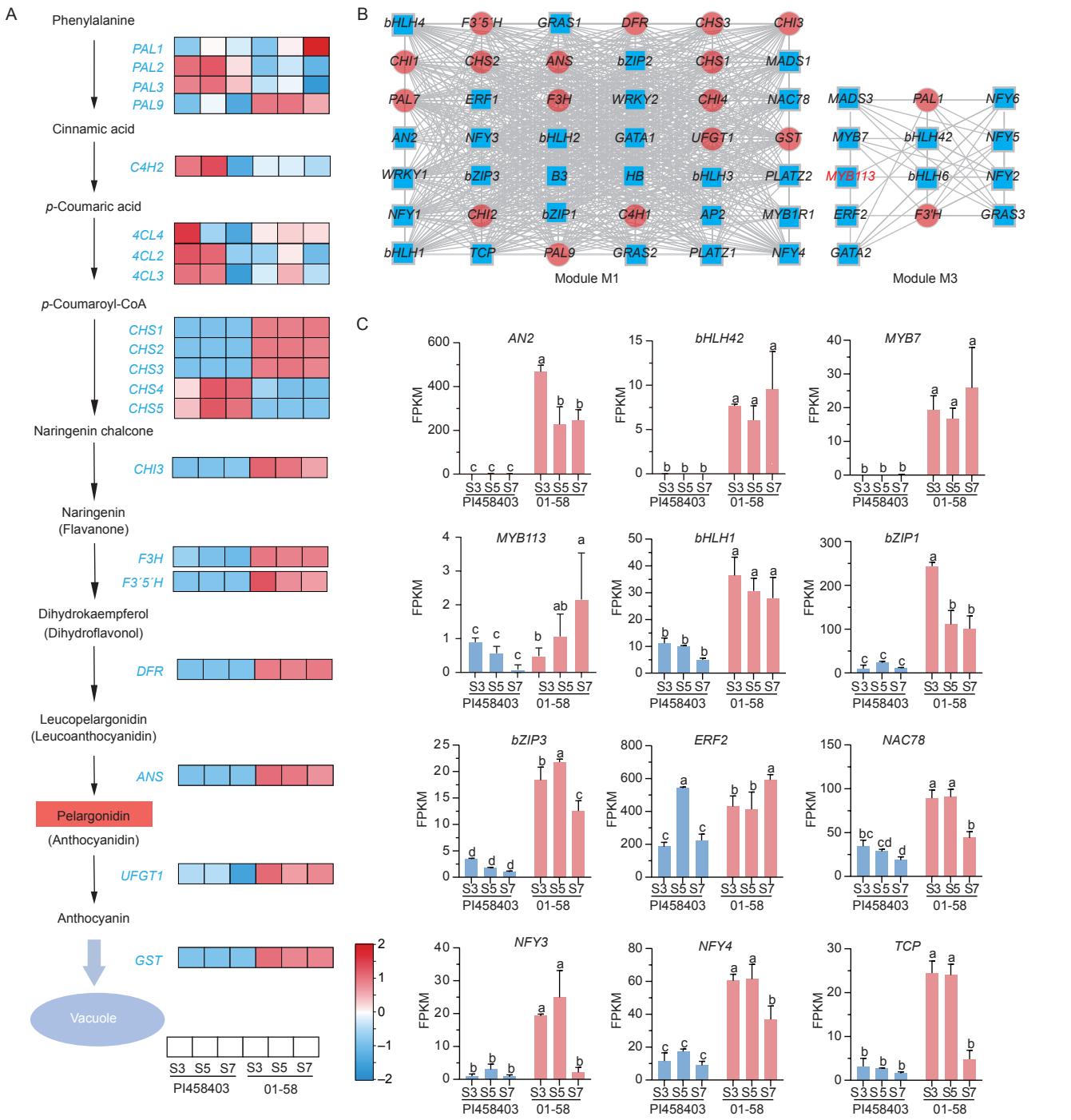


Fig. 6 Identification of candidate genes related to phenylpropanoid biosynthesis dynamics. A, heatmap represents the expression levels of biosynthetic pathway genes related to phenylpropanoids. The color gradient conveys the levels of the FPKM values. B, candidate genes with putative function related to phenylpropanoid biosynthesis and transcription. Red circles represent known genes identified previously, while blue rectangles indicate novel candidates identified in this study. C, expression changes of candidate differentially expressed genes related to phenylpropanoid pathway regulation identified from modules M1 and M3. Data are mean±SD (*n*=3). The letters denote the distinctions in mean gene expression across samples, as determined through Tukey's test.

protein (bHLH), basic region leucine zipper (bZIP), ethylene-responsive factor (ERF), GATA type zinc finger (GATA), Gibberellic Acid Insensitive-Repressor of GAI-Scarecrow (GRAS), homeobox-leucine zipper protein (HB), MADS, MYB, NAC domain-containing protein (NAC), nuclear transcription factor Y (NF-Y), plant AT-rich sequence and zinc-binding protein (PLATZ), *teosinte branched 1/cycloidea/proliferating cell factor* (TCP), and WRKY (Fig. 6-B). Consistent with the known MYB-bHLH-WD40 regulatory model (Liu *et al.* 2016, 2023; Strygina *et al.* 2019), we confirmed that TFs *AN2* and *bHLH42* had higher expression in 01-58 (FC≥2 and FDR<0.05) (Appendix L; Fig. 6-C). We also identified 10 additional TFs, including *MYB7*, *MYB113*, *bHLH1*, *bZIP1*/*3*, *ERF2*, *NAC78*, *NFY3*/*4*, and *TCP*, with significant

upregulation in 01-58 across at least two stages (Fig. 6-C). These TFs represent novel candidate regulators of the phenylpropanoid pathway warranting further investigation.

3.9. Functional validation of the candidate TF *StMYB113*

To functionally test a candidate gene, we selected *StMYB113*, a homolog of known anthocyanin regulators (Appendix M), for overexpression in potato (*MYB113*OE) (Fig. 7-A). Metabolomic profiling of two independent *MYB113*OE lines revealed 13 commonly upregulated DAMs compared to WT tubers (Fig. 7-B). Eight of these were phenolic acids, including hydroxycinnamic, hydroxybenzoic, and p-coumaroyl quinic acid derivatives (Fig. 7-C; Appendix N). Transcriptomic analysis identified 541 commonly upregulated DEGs in both transgenic lines (Fig. 7-D; Appendix O). KEGG enrichment of these DEGs showed a marked activation of the phenylpropanoid biosynthesis pathway (P=5.3×10^{-19}; Appendix P). Specifically, we identified five phenylpropanoid-related genes — *PAL1*, *PAL2*, *PAL4*, *HCT*, and *C3H-like*, — that were significantly induced in the *MYB113*OE lines (Fig. 7-E). Since *HCT* and *C3H-like* catalyze the redirection of metabolic flux toward phenolic acids, these transcriptional changes are consistent with the observed metabolite accumulation. These results demonstrate that *StMYB113* positively regulates phenolic acid biosynthesis by activating key genes in the phenylpropanoid pathway.

4. Discussion

In this study, we addressed the dynamic metabolic and transcriptional shifts during tuber swelling by profiling two distinct potato accessions. We successfully identified six stage-specific and four genotype-specific metabolite accumulation patterns, revealing the complex and dynamic nature of the tuber metabolome. By focusing on SGAs and phenylpropanoids, which showed the most conspicuous differences, we pinpointed a suite of novel candidate

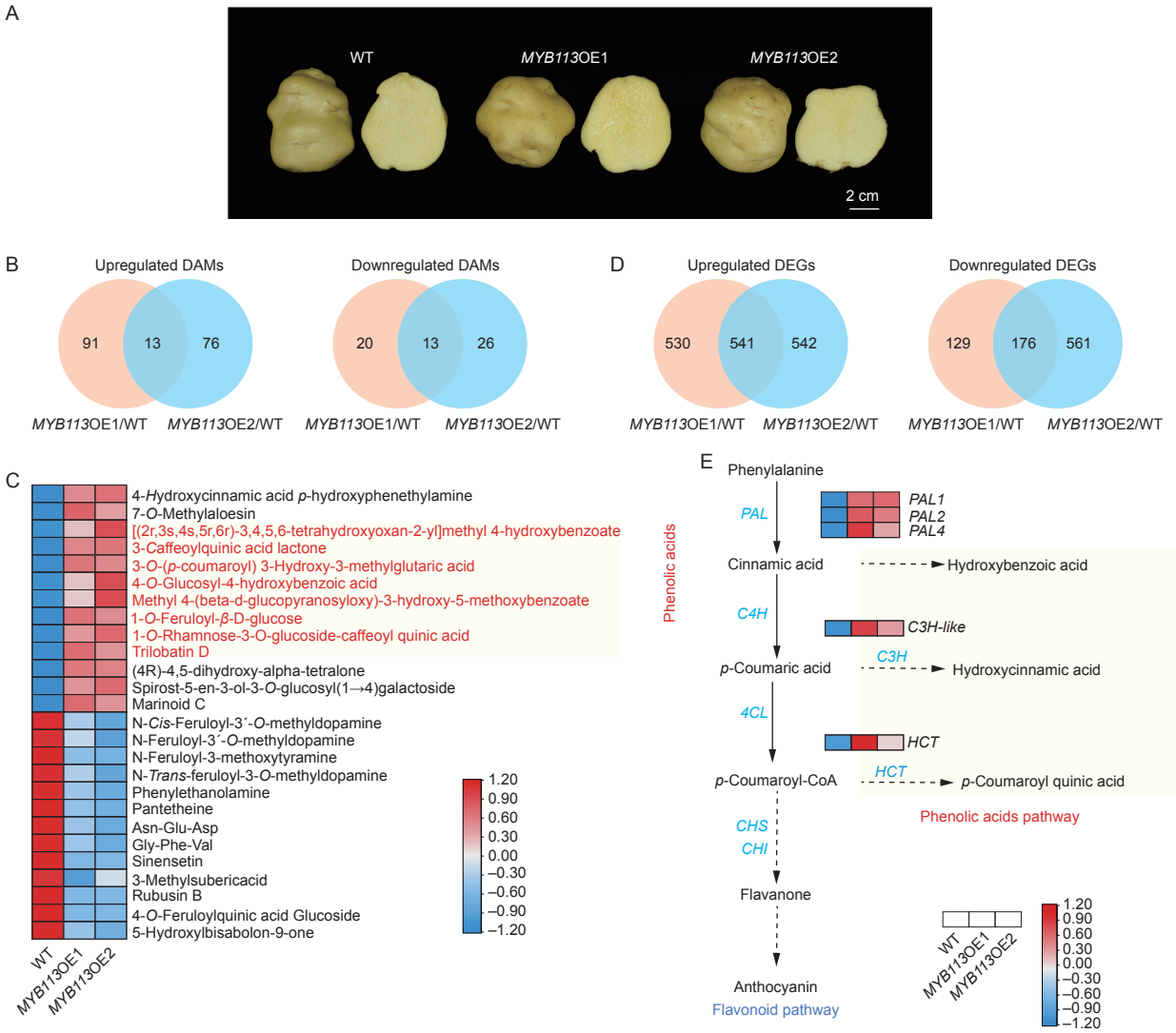


Fig. 7 Functional identification of StMYB113 in regulating phenolic acid metabolism in tuber flesh. A, morphological character of tubers from wild type (WT) and *MYB113* overexpressed (*MYB113*OE) line. B, overlap of DAMs between WT and *MYB113*OE lines. C, heatmap cluster of DAMs induced by *MYB113* overexpression in tuber flesh. D, overlap of DEGs between WT and *MYB113*OE lines. E, changes in the expression of genes involved in phenylpropanoids metabolism pathway between WT and *MYB113*OE lines.

biosynthetic genes and transcriptional regulators. These findings provide crucial insights into the mechanisms governing metabolic synthesis and regulation in developing tubers, directly addressing a key knowledge gap in potato biology.

The two accessions exhibited distinct temporal metabolic strategies. In the wild genotype PI458403, lipid metabolism dominated early development, reflecting the critical role of lipids in membrane remodeling and stress signaling during tuber early swelling (Okazaki and Saito 2014). For instance, phospholipid degradation may facilitate energy mobilization during tuber early swelling, whereas sphingolipid fluctuations can modulate pathogen defence (Cenzano *et al.* 2008; Ali *et al.* 2018). The subsequent shift to phenolic acid accumulation in later stages suggests a phased activation of defense mechanisms (Mandal *et al.* 2010; Sharma *et al.* 2019; González-Moreno *et al.* 2022). In contrast, the cultivated genotype 01-58 showed dynamic shifts in phenolic acid, flavonoids, and amino acids throughout development. Amino acids and their derivatives are essential for plant signal transduction and stress resistance enhancement, and serve as precursors for various secondary metabolites (Häusler *et al.* 2014; Cai and Aharoni 2022). Secondary metabolites, such as flavonoids and phenolic acids, also play roles as antioxidants, UV protection, and disease resistance, and they contribute to plant growth regulation and anthocyanin synthesis (Mandal *et al.* 2010; Shen *et al.* 2022; Rao and Zheng 2025). These divergent metabolic trajectories underscore the complex adaptations of wild and cultivated potatoes to their respective environmental and developmental pressures.

Despite developmental fluctuations, the metabolic differences between the accessions were far more pronounced. Consistent with selection during domestication, 01-58 showed significantly reduced SGA levels compared to PI458403 (Johns and Alonso 1990; Peng *et al.* 2019). Our expression analysis confirmed that this reduction was linked to the coordinated downregulation of SGA biosynthesis genes. Notably, the expression of the key transcription factor *StGAME9* was significantly suppressed in 01-58. A previous study showed that it could directly bind to or form a complex with *StMYC2* to regulate SGA biosynthesis genes such as *C5-SD*, thereby affecting SGA biosynthesis (Cárdenas *et al.* 2016). As *GAME9* is a known domestication target that regulates SGA biosynthesis genes (Hardigan *et al.* 2017), we propose its suppressed expression is a primary driver for the reduced SGA pathway activity observed in cultivated potatoes.

Beyond known regulators, our WGCNA identified novel candidate genes for SGA biosynthesis and modification. We identified four differentially expressed *cytochrome P450s* (*CYP71A1*, *CYP72A1/2/3*), likely catalyze key oxidation reactions. Among them, *CYP72* was homologous to *GAME6* (Umemoto *et al.* 2016), and may play a role in modifying SGA structures. Similarly, we identified a candidate *BAHD acyltransferase*, a family known for structural modification (Sonawane *et al.* 2023; Xie *et al.* 2024) and five new *zeatin-O-glucosyltransferases* (*ZOGs*) co-expressed with SGA biosynthetic genes (Wolters *et al.* 2023). These newly identified candidates, homologous to genes with established roles in SGA chemistry, represent promising targets for understanding the full complexity of this pathway.

In the phenylpropanoid pathway, the higher accumulation of pelargonidin derivatives in 01-58, which confers its red flesh (Zhang *et al.* 2023) was correlated with the significant upregulation of downstream genes like *DFR*, *ANS*, and *UFGT1*. This confirms their positive regulatory role in tuber pigmentation. Interestingly, several upstream genes (*PAL2/3*, *C4H2*, *CHS4/5*) were downregulated in 01-58, suggesting their metabolic flux may be preferentially directed toward other branch pathways, such as different phenolic acids. Our network analysis also identified 39 TFs potentially regulating the phenylpropanoid pathway. While we confirmed the upregulation of known regulators like *AN2* and *bHLH42* in 01-58, which has been reported as a positive core regulatory complex of anthocyanins in potatoes (Liu *et al.* 2016; Du *et al.* 2025). Our study uncovered a novel function for *StMYB113*. We demonstrated that it positively regulates phenolic acid biosynthesis in tuber flesh, a distinct role from its previously reported light-induced regulation of anthocyanins in the skin of a different potato cultivar (Zhang *et al.* 2024). Other transcription factors, including *bZIP*, *ERF*, *NAC*, *NFY*, and *TCP* were also notably upregulated in 01-58. The *bZIP1* is homologous to *VvibZIPC22*, and a previous study has shown that overexpression of *VvibZIPC22* in tobacco significantly increases the levels of kaempferol, quercetin 3-rutinoside, and cyanidin 3-rutinoside (Malacarne *et al.* 2016). *ERFs* have also been shown to influence flavonoid content by directly activating structural genes or interacting with *MYB* or MBW complexes. For instance, *ERF2* is homologous to *DcERF2*, which can upregulate the activity of *DcPAL3* promoter to enhance anthocyanin synthesis (Kimura *et al.* 2008). Moreover, *NAC78* is homologous to *ANAC078*, and overexpression or knockout of *ANAC078* increases or decreases the transcription of genes related to flavonoid biosynthesis, respectively (Morishita *et al.* 2009). These findings not only validate our multi-omics approach but also provide a rich list of novel, functionally supported candidates for future research into the intricate regulation of tuber quality traits.

5. Conclusion

This study integrated multi-omics datasets to construct a map of the metabolic and transcriptional changes governing potato tuber development. We elucidated the core genetic and regulatory networks controlling the biosynthesis of SGAs and phenylpropanoids, thereby explaining the key metabolic differences between wild and cultivated potatoes. The identification of numerous novel candidate genes, underscored by the functional validation of *StMYB113*'s previously unknown role in phenolic acid metabolism, represents a significant contribution to the field. These findings provide a valuable toolkit of high-confidence targets for the genetic improvement of potato, enabling breeders to precisely enhance nutritional value while reducing anti-nutritional compounds. Future studies should focus on the functional characterization of the other promising candidate

regulators identified here to fully harness their potential for improving tuber quality in breeding programs.

Acknowledgements

This work was financially supported by the Guangdong Major Project of Basic and Applied Basic Research, China (2021B03 01030004), the National Natural Science Foundation of China (32272725, 32488302), and the China Postdoctoral Science Foundation (2022M723463).

Declaration of competing interest

The authors declare that they have no conflict of interest.

Declaration of generative AI and AI-assisted technologies in the writing process

During the preparation of this manuscript, the authors used Hunyuan AI to assist in improving the clarity and readability of the language. All content generated was carefully reviewed and revised by the authors as necessary, and the authors take full responsibility for the final content of the article.

Appendices associated with this paper are available at https://doi.org/10.1016/j.jia.2025.12.070

References

Afnan Saleem A, Akhtar M F, Sharif A, Akhtar B, Siddique R, Ashraf G M, Alghamdi B S, Alharthy S A. 2022. Anticancer, cardio-protective and anti-inflammatory potential of natural-sources-derived phenolic acids. *Molecules*, **27**, 7286.

Akiyama R, Umemoto N, Mizutani M. 2023. Recent advances in steroidal glycoalkaloid biosynthesis in the genus *Solanum*. *Plant Biotechnology*, **40**, 185–191.

Al-Khayri J M, Sahana G R, Nagella P, Joseph B V, Alessa F M, Al-Mssallem M Q. 2022. Flavonoids as potential anti-inflammatory molecules: A review. *Molecules*, **27**, 2901.

Ali U, Li H, Wang X, Guo L. 2018. Emerging roles of sphingolipid signaling in plant response to biotic and abiotic stresses. *Molecular Plant*, **11**, 1328–1343.

Bao H, Yuan L, Luo Y, Jing X, Zhang Z, Wang J, Zhu G. 2024. A freezing responsive UDP-glycosyltransferase improves potato freezing tolerance via modifying flavonoid metabolism. *Horticultural Plant Journal*, **11**, 1595–1606.

Cai J, Aharoni A. 2022. Amino acids and their derivatives mediating defense priming and growth tradeoff. *Current Opinion in Plant Biology*, **69**, 102288.

Cárdenas P D, Sonawane P D, Heinig U, Jozwiak A, Panda S, Abebie B, Kazachkova Y, Pliner M, Unger T, Wolf D, Ofner I, Vilaprinyo E, Meir S, Davydov O, Gal-on A, Burdman S, Giri A, Zamir D, Scherf T, Szymanski J, *et al.* 2019. Pathways to defense metabolites and evading fruit bitterness in genus *Solanum* evolved through 2-oxoglutarate-dependent dioxygenases. *Nature Communications*, **10**, 5169.

Cárdenas P D, Sonawane P D, Pollier J, Vanden Bossche R, Dewangan V, Weithorn E, Tal L, Meir S, Rogachev I, Malitsky S, Giri A P, Goossens A, Burdman S, Aharoni A. 2016. *GAME9* regulates the biosynthesis of steroidal alkaloids and upstream isoprenoids in the plant mevalonate pathway. *Nature Communications*, **7**, 10654.

Cenzano A, Cantoro R, Racagni G, De Los Santos-Briones C, Hernández-Sotomayor T, Abdala G. 2008. Phospholipid and phospholipase changes by jasmonic acid during stolon to tuber transition of potato. *Plant Growth Regulation*, **56**, 307–316.

D'Amelia V, Aversano R, Batelli G, Caruso I, Castellano Moreno M, Castro-Sanz A B, Chiaiese P, Fasano C, Palomba F, Carputo D. 2014. High *AN1* variability and interaction with basic helix-loop-helix co-factors related to anthocyanin biosynthesis in potato leaves. *The Plant Journal*, **80**, 527–540.

Deng Y, Lu S. 2017. Biosynthesis and regulation of phenylpropanoids in plants. *Critical Reviews in Plant Sciences*, **36**, 257–290.

Du H, Zhai Z, Pu J, Liang J, Wang R, Zhang Z, Wang P, Zhu Y, Huang L, Li D, Chen K, Zhu G, Zhang C. 2025. Two tandem R2R3 MYB transcription factor genes cooperatively regulate anthocyanin accumulation in potato tuber flesh. *Plant Biotechnology Journal*, **23**, 1521–1534.

González Moreno A, de Cózar A, Prieto P, Domínguez E, Heredia A. 2022. Radiationless mechanism of UV deactivation by cuticle phenolics in plants. *Nature Communications*, **13**, 1786.

Hardigan M A, Laimbeer F P E, Newton L, Crisovan E, Hamilton J P, Vaillancourt B, Wiegert-Rininger K, Wood J C, Douches D S, Farré E M, Veilleux R E, Buell C R. 2017. Genome diversity of tuber-bearing *Solanum* uncovers complex evolutionary history and targets of domestication in the cultivated potato. *Proceedings of the National Academy of Sciences of the United States of America*, **114**, E9999–E10008.

Häusler R E, Ludewig F, Krueger S. 2014. Amino acids — A life between metabolism and signaling. *Plant Science*, **229**, 225–237.

Jia H, Xu Y, Deng Y, Xie Y, Gao Z, Lang Z, Niu Q. 2024. Key transcription factors regulate fruit ripening and metabolite accumulation in tomato. *Plant Physiology*, **195**, 2256–2273.

Johns T, Alonso J G. 1990. Glycoalkaloid change during the domestication of the potato, *Solanum* section *Petota*. *Euphytica*, **50**, 203–210.

Kang S, Wang F. 2024. Key players in plant defense: How scaffold protein GAME15 orchestrates the biosynthesis of steroidal defense metabolite. *Advanced Agrochem*, **4**, 10–12.

Kim D, Paggi J M, Park C, Bennett C, Salzberg S L. 2019. Graph-based genome alignment and genotyping with HISAT2 and HISAT-genotype. *Nature Biotechnology*, **37**, 907–915.

Kimura S, Chikagawa Y, Kato M, Maeda K, Ozeki Y. 2008. Upregulation of the promoter activity of the carrot (*Daucus carota*) phenylalanine ammonia-lyase gene (*DcPAL3*) is caused by new members of the transcriptional regulatory proteins, *DcRERF1* and *DcERF2*, which bind to the GCC-box homolog and act as an activator to the *DcPAL3* promoter. *Journal of Plant Research*, **121**, 499–508.

Langfelder P, Horvath S. 2008. WGCNA: An R package for weighted correlation network analysis. *BMC Bioinformatics*, **9**, 559.

Li Y, Chen Y, Zhou L, You S, Deng H, Chen Y, Alseekh S, Yuan Y, Fu R, Zhang Z, Su D, Fernie A R, Bouzayen M, Ma T, Liu M, Zhang Y. 2020. MicroTom metabolic network: Rewiring tomato metabolic regulatory network throughout the growth cycle. *Molecular Plant*, **13**, 1203–1218.

Liu Y, Li Y, Liu Z, Wang L, Lin-Wang K, Zhu J, Bi Z, Sun C, Zhang J, Bai J. 2023. Integrative analysis of metabolome and transcriptome reveals a dynamic regulatory network of potato tuber pigmentation. *iScience*, **26**, 105903.

Liu Y, Kui L W, Espley R V, Wang L, Yang H, Yu B, Dare A, Varkonyi-Gasic E, Wang J, Zhang J, Wang D, Allan A C. 2016. Functional diversification of the potato R2R3 MYB anthocyanin activators *AN1*, *MYBA1*, and *MYB113* and their interaction with basic helix-loop-helix cofactors. *Journal of Experimental Botany*, **67**, 2159–2176.

Lucier R, Kamileen M O, Nakamura Y, Serediuk S, Barbole R, Wurlitzer J, Kunert M, Heinicke S, O'Connor S E, Sonawane P D. 2024. Steroidal scaffold decorations in *Solanum* alkaloid biosynthesis. *Molecular Plant*, **17**, 1236–1254.

Luo J, He C, Yan S, Jiang C, Chen A, Li K, Zhu Y, Gui S, Yang N, Xiao Y, Wu S, Zhang F, Liu T, Wang J, Huang W, Yang Y, Wang H, Yang W, Li W, Zhuo L, *et al.* 2024. A metabolic roadmap of waxy corn flavor. *Molecular Plant*, **17**, 1883–1898.

Malacarne G, Coller E, Czemmel S, Vrhovsek U, Engelen K, Goremykin V, Bogs J, Moser C. 2016. The grapevine *VvibZIPC22* transcription factor is involved in the regulation of flavonoid biosynthesis. *Journal of Experimental Botany*, **67**, 3509–3522.

Mandal S M, Chakraborty D, Dey S. 2010. Phenolic acids act as signaling molecules in plant-microbe symbioses. *Plant Signaling & Behavior*, **5**, 359–368.

Mao J, Gao Z, Wang X, Lin M, Chen L, Ning X. 2024. Combined widely targeted metabolomic, transcriptomic, and spatial metabolomic analysis reveals the potential mechanism of coloration and fruit quality formation in *Actinidia chinensis* cv. Hongyang. *Foods*, **13**, 233.

Mattioli R, Francioso A, Mosca L, Silva P. 2020. Anthocyanins: A

comprehensive review of their chemical properties and health effects on cardiovascular and neurodegenerative diseases. *Molecules*, **25**, 3809.

Morishita T, Kojima Y, Maruta T, Nishizawa-Yokoi A, Yabuta Y, Shigeoka S. 2009. *Arabidopsis* NAC transcription factor, *ANAC078*, regulates flavonoid biosynthesis under high-light. *Plant and Cell Physiology*, **50**, 2210–2222.

Okazaki Y, Saito K. 2014. Roles of lipids as signaling molecules and mitigators during stress response in plants. *The Plant Journal*, **79**, 584–596.

Peng Z, Wang P, Tang D, Shang Y, Li C, Huang S, Zhang C. 2019. Inheritance of steroidal glycoalkaloids in potato tuber flesh. *Journal of Integrative Agriculture*, **18**, 2255–2263.

Rao M J, Zheng B. 2025. The role of polyphenols in abiotic stress tolerance and their antioxidant properties to scavenge reactive oxygen species and free radicals. *Antioxidants*, **14**, 74.

Shannon P, Markiel A, Ozier O, Baliga N S, Wang J T, Ramage D, Amin N, Schwikowski B, Ideker T. 2003. Cytoscape: A software environment for integrated models of biomolecular interaction networks. *Genome Research*, **13**, 2498–2504.

Sharma A, Shahzad B, Rehman A, Bhardwaj R, Landi M, Zheng B. 2019. Response of phenylpropanoid pathway and the role of polyphenols in plants under abiotic stress. *Molecules*, **24**, 2452.

Shen N, Wang T, Gan Q, Liu S, Wang L, Jin B. 2022. Plant flavonoids: Classification, distribution, biosynthesis, and antioxidant activity. *Food Chemistry*, **383**, 132531.

Sonawane P D, Gharat S A, Jozwiak A, Barbole R, Heinicke S, Almekias-Siegl E, Meir S, Rogachev I, Connor S E O, Giri A P, Aharoni A. 2023. A BAHD-type acyltransferase concludes the biosynthetic pathway of non-bitter glycoalkaloids in ripe tomato fruit. *Nature Communications*, **14**, 4540.

Sonawane P D, Jozwiak A, Barbole R, Panda S, Abebie B, Kazachkova Y, Gharat S A, Ramot O, Unger T, Wizler G, Meir S, Rogachev I, Doron-Faigenboim A, Petreikov M, Schaffer A, Giri A P, Scherf T, Aharoni A. 2022. 2-oxoglutarate-dependent dioxygenases drive expansion of steroidal alkaloid structural diversity in the genus *Solanum*. *New Phytologist*, **234**, 1394–1410.

Song Z, Xu X, Chen X, Chang J, Li J, Cheng J, Zhang B. 2024. Multi-omics analysis provides insights into the mechanism underlying fruit color formation in *Capsicum*. *Frontiers in Plant Science*, **15**, 1448060.

Strygina K V, Kochetov A V, Khlestkina E K. 2019. Genetic control of anthocyanin pigmentation of potato tissues. *BMC Genetics*, **20**, 27.

Tai H H, Worrall K, Pelletier Y, De Koeyer D, Calhoun L A. 2014. Comparative metabolite profiling of *Solanum tuberosum* against six wild *Solanum* species with colorado potato beetle resistance. *Journal of Agricultural and Food Chemistry*, **62**, 9043–9055.

Umemoto N, Nakayasu M, Ohyama K, Yotsu-Yamashita M, Mizutani M, Seki H, Saito K, Muranaka T. 2016. Two cytochrome P450 monooxygenases catalyze early hydroxylation steps in the potato steroid glycoalkaloid biosynthetic pathway. *Plant Physiology*, **171**, 2458–2467.

Wang C, Meng L, Gao Y, Grierson D, Fu D. 2018. Manipulation of light signal transduction factors as a means of modifying steroidal glycoalkaloids accumulation in tomato leaves. *Frontiers in Plant Science*, **9**, 437.

Wang R, Shu P, Zhang C, Zhang J, Chen Y, Zhang Y, Du K, Xie Y, Li M, Ma T, Zhang Y, Li Z, Grierson D, Pirrello J, Chen K, Bouzayen M, Zhang B, Liu M. 2022. Integrative analyses of metabolome and genome-wide transcriptome reveal the regulatory network governing flavor formation in kiwifruit (*Actinidia chinensis*). *New Phytologist*, **233**, 373–389.

Wolters P J, Wouters D, Tikunov Y M, Ayilalath S, Kodde L P, Strijker M F, Caarls L, Visser R G F, Vleeshouwers V G. 2023. Tetraose steroidal glycoalkaloids from potato provide resistance against *Alternaria solani* and Colorado potato beetle. *eLife*, **12**, RP87135.

Xie Y, Xu Y, Jia H, Wang K, Chen S, Ma T, Deng Y, Lang Z, Niu Q. 2024. Tomato *MADS-RIN* regulates *GAME5* expression to promote non-bitter glycoalkaloid biosynthesis in fruit. *The Plant Journal*, **120**, 2500–2514.

Xu J, Yan J, Li W, Wang Q, Wang C, Guo J, Geng D, Guan Q, Ma F. 2020. Integrative analyses of widely targeted metabolic profiling and transcriptome data reveals molecular insight into metabolomic variations during apple (*Malus domestica*) fruit development and ripening. *International Journal of Molecular Sciences*, **21**, 4797.

Yang X, Zhang L, Guo X, Xu J, Zhang K, Yang Y, Yang Y, Jian Y, Dong D, Huang S, Cheng F, Li G. 2023. The gap-free potato genome assembly reveals large tandem gene clusters of agronomical importance in highly repeated genomic regions. *Molecular Plant*, **16**, 314–317.

Ye M, Peng Z, Tang D, Yang Z, Li D, Xu Y, Zhang C, Huang S. 2018. Generation of self-compatible diploid potato by knockout of *S-RNase*. *Nature Plants*, **4**, 651–654.

Zhang Z, Shi Q, Wang B, Ma A, Wang Y, Xue Q, Shen B, Hamaila H, Tang T, Qi X, Fernie A R, Luo J, Li X. 2022. Jujube metabolome selection determined the edible properties acquired during domestication. *The Plant Journal*, **109**, 1116–1133.

Zhang Z, Zhou D, Li S, Pan J, Liang J, Wu X, Wu X N, Krall L, Zhu G. 2023. Multi-omics analysis reveals the chemical and genetic bases of pigmented potato tuber. *Journal of Agricultural and Food Chemistry*, **71**, 16402–16416.

Zhang Z, Zhou J, Zhao Y, Zhao X, Liu J, Liu J, Zhang J, Song B, Zhang H. 2024. *StMYB113* promotes anthocyanin biosynthesis in potato (*Solanum tuberosum* L.) désirée tubers. *Potato Research*, **67**, 307–324.

Zhao L, Zhang B, Huang H, Huang W, Zhang Z, Wang Q, Luo H, An B. 2023. Metabolomic and transcriptomic analyses provide insights into metabolic networks during cashew fruit development and ripening. *Food Chemistry*, **404**, 134765.

Zhao X, Zhang H, Liu T, Zhao Y, Hu X, Liu S, Lin Y, Song B, He C. 2023a. Transcriptome analysis provides *StMYBA1* gene that regulates potato anthocyanin biosynthesis by activating structural genes. *Frontiers in Plant Science*, **14**, 1087121.

Zhao X, Zhang Y, Lai J, Deng Y, Hao Y, Wang S, Yang J. 2023b. The *SlDOG1* affect biosynthesis of steroidal glycoalkaloids by regulating *GAME* expression in tomato. *International Journal of Molecular Sciences*, **24**, 3360.

Zhu Z, Wei L, Guo L, Bao H, Wang X, Kear P, Wang Z, Zhu G. 2023. Integrated full-length transcriptome and metabolome profiling reveals flavonoid regulation in response to freezing stress in potato. *Plants*, **12**, 2054.

Executive Editor-in-Chief Sanwen Huang
Managing Editor Lingyun Weng